Int. J. Heat Mass Transfer. Vol. 21, pp. 285–294. Pergamon Press 1978. Printed in Great Britain

TRANSPORT CHARACTERISTICS OF FILMS FLOWING OVER HORIZONTAL SMOOTH TUBES*

S. SIDEMAN, H. HORN and D. MOALEM†
Department of Chemical Engineering, Technion—Israel Institute of Technology, Haifa, Israel

(*Received* 4 *February* 1977)

Abstract—An electrochemical technique, utilizing potassium ferrocyanide–potassium ferricyanide solution, provided reliable instantaneous local transfer rates between a film and a horizontal tube. Analog–digital conversion enabled a detailed analysis of the local, spatial and temporal transfer characteristics.

The transfer rate was found to depend on the mode of liquid feeding. Depending upon the range of flow rates and distance between the test-tube and the liquid feeding tube, four characteristic transfer regimes were identified: (1) continuous smooth film flow between the tubes, (2) rivulated film flow, (3) dripping between tubes, (4) continuous jets flowing between the tubes. Dripping between the tubes was found to enhance the transfer rate by a factor of two as compared to smooth film feeding.

A theoretical analysis gave good agreement with the experimental data for the lower bound smooth film flow and the upper bound dripping phenomena.

NOMENCLATURE

B, dimensionless parameter ($= ReFr$);
C, concentration, molar;
d, diameter;
D, molecular diffusivity of solute;
$\mathscr{D}$, dimensionless molecular diffusivity ($= D/Ru_r$);
F, frequency;
Fr, Froude number ($= gR/u_r^2$);
g, gravitation constant;
H, vertical distance between two adjacent tubes;
K, temporal and spatial mean transfer coefficient;
k, instantaneous local mass-transfer coefficient;
k_x, local mass-transfer coefficient;
L_0, ratio of concentration to momentum boundary layer thickness of stagnation region, equations (18) and (25);
R, radius of tube;
Re, Reynolds number ($= Ru_r\rho/\mu$); $Re_N = 4\Gamma/\mu$;
$\mathbf{r}$, radius vector;
S, slope of velocity profile at the wall, equation (9);
Sc, Schmidt number ($= \nu/D$);
Sh_x, Sherwood number ($= k_xR/D$);
U, local dimensionless velocity ($= u/u_r$);
$\bar{U}$, local mean dimensionless velocity [equation (8a)];
u, local x-directed velocity;
u_r, reference velocity, arbitrary;
u_p, potential velocity in stagnation region;
u_t, free stream approach velocity;
u_∞, free stream approach velocity;
X, dimensionless coordinate ($= x/R$);
x, tangential coordinate, peripheral distance from stagnation point;
x_0, distance from $x = 0$; end of stagnation region;
Y, dimensionless normal coordinate ($= y/R$);
y, normal coordinate;
y_f, film thickness.

Greek symbols

Γ, half liquid mass flow rate of film, per unit tube length;
$\delta_{c,0}$, dimensionless concentration boundary-layer thickness at $x = x_0$;
δ_c, dimensionless concentration boundary-layer thickness (y/R);
δ_f, dimensionless film thickness ($= y_f/R$);
δ_m, dimensionless momentum boundary-layer thickness;
λ, distance between active dripping sites;
θ, angle from the vertical;
θ_r, local slope of radius vector;
μ, viscosity;
ν, kinematic viscosity;
ρ, density;
ψ, dimensionless concentration, equation (3);
ω, dimensionless bulk flow rate ($= \Gamma/u_r\rho R$), equation (8b).

Subscripts

b, bulk;
c, concentration, mass;
f, film (thickness);
m, momentum;
0, initial;
w, wall.

*Presented 69th Annual AIChE Meeting, Chicago, IL, December 1976.

†School of Engineering, Department of Fluid Mechanics and Heat Transfer, Tel-Aviv University, Tel-Aviv, Israel.

INTRODUCTION

HEAT and mass transfer across thin liquid films occur in a wide spectrum of engineering applications such as packed columns, wetted wall columns, suspended wetted plates or wires, rectification equipment, etc. Extensive use of thin film flow is made in various film-type heat-exchangers, such as vapor condensers and film evaporators. These show the distinct advantage of high heat transfer coefficients and are utilized in various water desalination units.

This work comes, in a way, to complement an earlier theoretical and experimental study on a film-type evaporator–condenser where condensation takes place inside a horizontal tube bundle while the cooling evaporating film flows over the outside of the tubes [1–4]. As is shown in these earlier studies, the overall transfer rate is controlled by the external evaporating film and is highly affected by the film flow characteristics.

The object of the present study was to elucidate the effect of the film flow characteristics and the mode of the liquid flow between the tubes, i.e. films, drops or jets, on the local, spatial and time average transfer coefficients. This information should provide a deeper insight into the physical phenomena and lead to better design and control over the governing parameters.

The results, obtained by cine-camera studies and measurements of the solid–liquid mass-transfer rates by an electrochemical technique, are reported herein. The data are in good agreement with the theoretical upper and lower bound solutions presented here.

THE EXPERIMENTAL SYSTEM

The electrochemical process used in the present investigation is the well-known [5] chemical reduction of ferricyanide ions at a nickel cathode. The presence of a large excess of an inert electrolyte (sodium hydroxide) negates the effects of ionic migration under the applied potential gradient.

Measurements are made of the mass transfer rate of the chemical species $Fe(CN)_6^{3-}$ (ferricyanide ion) from the bulk of the down flowing liquid film to the surface of a small, electrically isolated, cathode set flush with the outer surface of the tube section which forms the control cathode. The electro-chemical reaction which takes place at the surface results in the formation of a ferrocyanide ion, $Fe(CN)_6^{4-}$.

The control cathode, as well as the small measurement cathode inserted in it, are electrically connected to another section of the tube—an anode—which has a 100 times larger surface area. Here the reversed reaction occurs once the circuit is closed by the continuous liquid film. Essentially, the method involves the measurement of the current flowing in this electrochemical cell at the limiting current. The mass flux is then governed by the rate of molecular diffusion of the ferricyanide ions from the bulk solution to the cathode surface. Under these conditions the concentration of ferricyanide ion at the cathode surface is negligible compared with the bulk concentration and the measured current is independent of the applied potential.

Note that in the case of large Schmidt numbers, the naturally occurring surface roughness significantly influences the mass or heat transfer rate. The advantage of the electrochemical techniques is that surface roughness can be kept very small in comparison with the dissolving wall method.

Apparatus

A schematic diagram of the flow system is presented in Fig. 1. The experimental apparatus consists of a feeding system, the test cell and an electrical measuring circuit.

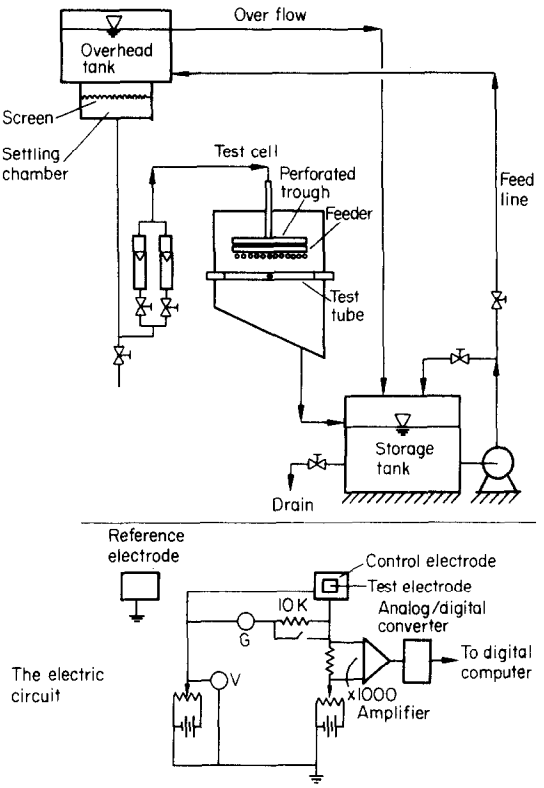

FIG. 1. Schematic diagrams of the experimental set-up.

The liquid employed in the experiments is made of equimolar, 0.01 g mole l^{-1} concentrations of potassium ferricyanide and potassium ferrocyanide in a 1.5 g mole l^{-1} solution of sodium hydroxide in distilled water. For this composition, $\mu = 1.59 \times 10^{-2}$ cP and $D = 10^{-5}$ cm^2 s^{-1}, (the physical properties of the solution are determined by the concentration of sodium hydroxide). Note that it is necessary to renew the solution once in a while due to the effect of sunlight on the complex ions in the solution.

The electrolyte solution was recirculated through ducts of vinyl chloride, utilizing a stainless steel pump. The liquid flow rate was measured by a set of rotameters, with polyvinyl chloride floats.

The test cell, made of Plexiglas, contains a perforated trough, which continuously wets a dummy "feeder" tube placed below it, thus simulating real flow

conditions for the test-tube situated under the feeder tube. The liquid flow rate and the vertical spacing between the tubes determine the mode of liquid distribution, i.e. films, drops or jets. The attainment of a uniform continuous film on the smooth nickel or nickel-plated test tube is imperative to the success of experimental investigation.

The cylindrical test-tube is 38 mm in diameter and approximately 300 mm long. It is made of a number of nickel (or nickel-plated brass) sections which are electrically isolated from each other. The control electrodes—the cathodes—are replaceable and can be machined to any shape. The test electrodes, 0.2 mm in diameter, are set at different points in the control electrodes, so that local mass fluxes can be measured.

The electric circuit consists of two independent power supply systems and of control and measuring devices which control and equilibrate the electrical potential of the cathodes. The voltage output is connected through an amplifier to a digital PDP computer for sampling and analyzing the collected data [6].

The remainder of the apparatus is conventional in design and serves to provide a metered, temperature controlled, liquid flow to the test section. A Bolex 16H cine camera was used throughout at 68 fps.

THEORETICAL

As will be shown below, the mode of the liquid flow between the tubes determine the solid–fluid mass-transfer rate. The liquid flow configuration between the tubes is determined by the flow rate and the vertical distance between the vertically adjacent tubes. For a small distance between the tubes, a continuous smooth film cascades from the upper to the lower tube. As the tube distance between the tubes increases, rivulating flow occurs and discontinuous fractions of the film, which seem to move horizontally in between the tubes, drain on to the lower tube. Further increasing the distance brings about the formation of drops. By increasing the flow rate, the trains of drops change to continuous jets.

The following analysis deals with the case where the liquid between the tubes is a smooth continuous film. As shown, this represents the lower bound solution. An upper bound solution, appropriate for the case of drops falling between the tubes, is then approximated.

(A) *Continuous film flow between tubes*

A schematic presentation of the physical model and the coordinates used here are shown in Fig. 2. Consistent with the physical conditions in which the experimental data were obtained, we neglect here the contribution of the terms of migration and convection normal to the reacting surface. Also, at the limiting current, the concentration at the surface of the electrode is zero.

The external surface of the tube is continually wetted by a ferricyanide solution with an initial molar concentration, C_0. This film, which is formed on the external side of the tube, is flowing in the x-direction along the perimeter and is draining at the bottom of the tube.

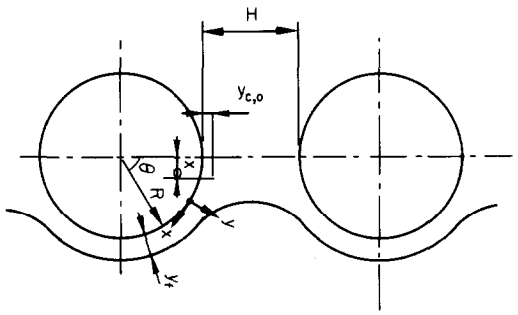

FIG. 2. Schematic diagrams of physical model.

Consider an angular cross-section $\Delta\theta$ at some distance x from the upper stagnation point. The thickness of the liquid film, y_f, is assumed to be small relative to the radius vector, **r**, so that Cartesian coordinates may conveniently be used. Hence, two dimensional film flow is locally considered along the periphery. The local angle of inclination varies with the peripheral distance x and equals the local slope of the radius vector.

The formulation of the governing equations can be simplified by stipulating that (a) the inertial terms are negligible as compared to gravitational forces, (b) the second derivatives of the velocities with respect to x are negligible as compared with the corresponding y-derivatives, (c) the tangential and normal pressure drop in the thin film are negligible and (d) that surface tension effect may be ignored. Consistent with the above assumption, the momentum equation reduces to:

$$\mu\frac{d^2u}{dy^2}+\rho g\sin\theta=0, \tag{1}$$

where u is local x-directed velocity. As the velocity of the film is y-dependent, the conservation of mass is expressed in integral form. Neglecting the molecular diffusion in the x-direction of flow, a mass balance on an element of Δx width and y_f height yields:

$$\frac{d}{dx}\int_0^{y_f}(C_b-C)u\,dy=D\left.\frac{dC}{dy}\right|_{y=0}, \tag{2}$$

where C is the local concentration; C_b is a bulk concentration outside the concentration boundary layer y_c, and D is the molecular mass diffusivity of solute. Taking the radius of the tube R as the characteristic length and u_r as an arbitrary reference velocity, we define the following dimensionless variables:

$$X=x/R;\quad Y=y/R;\quad \delta_f=y_f/R,$$
$$\psi=\frac{C-C_w}{C_b-C_w};\quad U=u/u_r, \tag{3}$$

where C_w is the wall concentration. Note that $C_b=C_0$ at $x=0$.

The dimensionless forms of the momentum and mass equations are:

$$\frac{d^2U}{dy^2} = -B\sin X; \qquad B = \left(\frac{gR}{u_r^2}\right)\cdot\left(\frac{\rho u_r R}{\mu}\right) = Fr\cdot Re, \tag{4}$$

$$\frac{d}{dX}\int_0^{\delta_c}(1-\psi)U\,dY = \mathscr{D}\left.\frac{d\psi}{dY}\right|_{y=0}; \quad \mathscr{D} = \frac{D}{Ru_r}, \tag{5}$$

where δ_c is the dimensionless thickness of the mass boundary layer ($=y_c/R$). The concentration profile is approximated, following Von-Karman's approach, by specifying the following boundary conditions:

$$\text{at } Y=\delta_c;\quad \psi = 1 \text{ and } \frac{d\psi}{dY} = 0$$

$$\text{at } Y = 0;\quad \psi = 0$$

$$\text{at } Y = 0;\quad \frac{d^2\psi}{dY^2} = 0.$$

The latter boundary condition is applicable for constant pressure conditions, with the axial and normal velocities being zero at the wall. The resulting mass distribution polynomial is given by:

$$\psi(Y) = \frac{3}{2}\frac{Y}{\delta_c} - \frac{1}{2}\left(\frac{Y}{\delta_c}\right)^2. \tag{6}$$

The velocity profile is derived by integrating the momentum equation, assuming the classical boundary conditions of no-slip velocity on the solid surface and zero shear stress on the free interface of the liquid film. This yields:

$$U = B\sin X\left(\delta_f Y - \frac{Y^2}{2}\right). \tag{7}$$

The local dimensionless mean velocity $\bar{U}$ and bulk flow rate (per unit length of tube) are, respectively:

$$\bar{U} = \tfrac{1}{3}\delta_f^2 B\sin X, \tag{8a}$$

$$\omega \equiv \frac{\Gamma}{u_r\rho R} = \tfrac{1}{3}\delta_f^3 B\sin X, \tag{8b}$$

where Γ is the (half) mass flow rate, per unit length of tube.

In the case under consideration, the Schmidt number is large ($>10^3$) and the resistance to mass transfer is located in the thin concentration boundary-layer. Hence, a linear velocity profile may reasonably be assumed

$$U = SY, \tag{9}$$

where S is the slope of the velocity profile at the wall. Differentiating equation (7) and rearranging yields:

$$S = (3B^2\sin^2 X)^{1/3} = \frac{3}{\delta_f^2}. \tag{10}$$

Substituting equations (6) and (9) in (5) and rearranging yields:

$$\delta_c^2\,d\delta_c = 7.5\frac{\mathscr{D}}{S}\,dX. \tag{11}$$

Integrating equation (11) between the appropriate limits, yields:

$$\tfrac{1}{3}(\delta_c^3 - \delta_{c,0}^3) = 7.5\frac{\mathscr{D}}{S}(X - X_0), \tag{12}$$

where $\delta_{c,0}$ denotes the initial concentration boundary-layer thickness at a distance $X = X_0$ from the stagnation point at the top of the tube.

For the model depicted in Fig. 2, and with $\delta_c \ll \delta_f$ associated with $Sc > 1000$, the value of $\delta_{c,0}$ at X_0 can be approximated by assuming "infinite" flow between the tubes. Under these conditions, the momentum boundary layer, $\delta_{m,0}$ and the free "potential" velocity in the stagnation region u_p are respectively given by [7].

$$\delta_{m,0} \equiv \frac{y_m}{R} = 2.4\sqrt{(\nu x/u_p)} = 2.4\sqrt{(\nu/u_1)}, \tag{13}$$

where

$$u_p = u_1 x \quad u_1 = \frac{2}{R}u_\infty, \quad u_\infty = \sqrt{(2gH)}. \tag{14}$$

Here, u_∞ is the free stream approach velocity and H is the vertical distance between the tubes. The value of $\delta_{c,0}$ is now approximated via Schlichting's [7] relationship for the local mass-transfer coefficient in the stagnation region, for $Sc \gg 1$, i.e.

$$\frac{k_x x}{D} = 0.339\left(\frac{\nu}{D}\right)^{1/3}\left(\frac{u_p x}{\nu}\right)^{1/2}, \tag{15}$$

where k_x, the local mass-transfer coefficient, is defined by

$$k_x(C_w - C_b) = -D\left.\frac{\partial C}{\partial y}\right|_{y=0}. \tag{16}$$

Differentiation of equation (6) and rearranging (16) yields

$$k_x = \frac{3D}{2y_c} = \frac{3D}{2R\delta_c}. \tag{17}$$

Introducing (17) and (14) into (15) and dividing by (13) yields the ratio of $\delta_{c,0}/\delta_{m,0}$ for the stagnation region:

$$L_0 = \frac{\delta_{c,0}}{\delta_{m,0}} = 1.844Sc^{-1/3}, \tag{18}$$

from which $\delta_{c,0}$ is evaluated. It is to be emphasized that equation (15) and the resulting equation (18) are appropriate only near the stagnation point, when $x_0 = 0$, whereas equation (17) applies for the whole circumference.

Introducing $\delta_{c,0}$ (and $x_0 = 0$) into (12), utilizing equations (9) and (8b), provides an expression for δ_c for the whole circumference:

$$\delta_c = \left[\frac{7.5\mathscr{D}X}{\omega^{1/3}}\left(\frac{3}{B\sin\theta}\right)^{2/3} + (L_0\delta_{m,0})^3\right]^{1/3} \tag{19}$$

Introducing (19) into (17) and rearranging yields:

$$k_x = \tfrac{3}{2}D\left[\frac{\Gamma}{7.5\rho D x y_f^2 + \Gamma y_{c,0}^3}\right]^{1/3}, \tag{20}$$

or, in terms of the local Sherwood number:

$$Sh_x = \frac{k_x R}{D} = \frac{3}{2}\left[\frac{\omega}{7.5\mathscr{D}X\left(\frac{3\omega}{B\sin\theta}\right)^{2/3} + \omega\left[4.43Sc^{-1/3}\sqrt{\left(\frac{\nu R}{u_\infty}\right)}\right]^3}\right]^{1/3}. \quad (21)$$

Finally, integration along the periphery yields the average transfer coefficient, K:

$$K = \frac{1}{\pi R}\int_0^{\pi R} k_x \, dX. \quad (22)$$

(B) *Approximate solution for the falling drops case*

Consider the lower horizontal tube continuously wetted by drops falling on it from a large number of dripping sites above it. The time interval between the successive drops falling at an average frequency f is much smaller than the time interval required for a complete drainage of the existing film. Furthermore, since $Sc \gg 1$ and $\delta_c \ll \delta_m$, the concentration boundary-layer thickness at the stagnation point is practically time independent. Under these conditions, one can approximate the effect of the falling drops on the top of the tube by solving for a corresponding effect of a falling sheet at the stagnation region. In other words, the cumulative effect of the drops which fall at random places along the top of the horizontal tube is approximated by solving for the integral effect of an orderly sheet falling along the tube with an identical average flow rate.

Under these assumptions, the above analysis for a continuous film flow between the tubes is applicable. However, unlike the "infinite" flow case, the stagnation region parameters are now approximated by utilizing the solution for a viscous boundary layer developing inside a two-dimensional jet impinging on a flat surface, yielding [8, 9]:

$$\delta_{m,0} = 2.4\nu\sqrt{\left(\frac{Re_N}{\pi g H}\right)}, \quad (23)$$

and

$$x_0 = \frac{\sqrt{2}}{\pi}\frac{\nu Re_N}{\sqrt{(gH)}}. \quad (24)$$

Consequently, the thickness ratio of the concentration to the momentum boundary layer is given by:

$$L_0 = \frac{\delta_{c,0}}{\delta_{m,0}} = 0.922Sc^{-1/3}\sqrt{\left(\frac{\pi R u_\infty}{\nu Re_N}\right)}, \quad (25)$$

which is now to be used in equations (19)–(22).

RESULTS AND DISCUSSION

As the mass transfer rates are mainly determined by the mode of the liquid flow between the consecutive horizontal tubes, the results will be related to "continuous" and "discontinuous" flows between the tubes.

(A) *Continuous flow between tubes*

When the tubes are closely spaced in the vertical direction, a continuous film cascades between the two tubes. Complete wetting of the circumference along the tube is obtained at $Re_N \simeq 100$. When operating under these conditions, the temporal variations of the flow and mass-transfer rates at any point along the circumference are negligible.

Figure 3 represents the calculated average mass-transfer coefficients as a function of the film Reynolds number Re_N for various values of the Schmidt number.

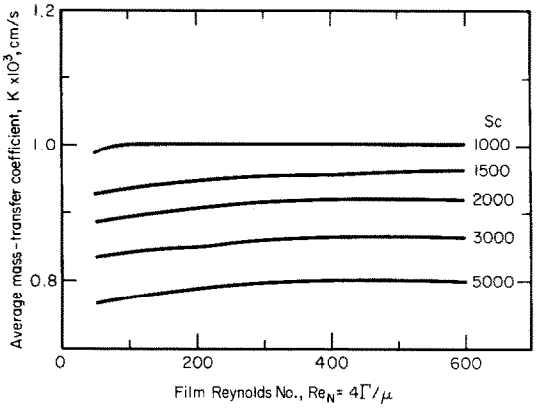

FIG. 3. Calculated average mass-transfer coefficients for continuous smooth film flow.

As is seen from Fig. 3, the film flow rate has but a small effect on the mass-transfer coefficient since, by equation (20), k_x is proportional to $Re_N^{1/9}$. The same functional dependence was also obtained by Kramers and Kreygel [10] and Oliver and Atherinos [11] in the solution of mass transfer from a flat surface into a laminar boundary layer in well-developed flow. These solutions, applied sectionally to the case at hand, are compared in Fig. 4 with equation (20) and the experimental data. As demonstrated in Fig. 4, the present analysis is in a better agreement with the data since it accounts for the proper initial value at the

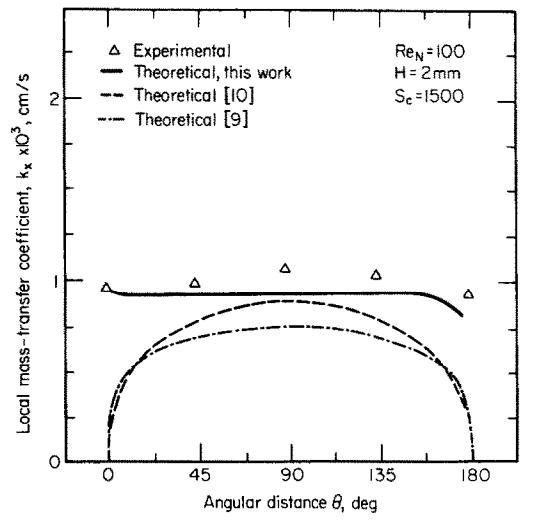

FIG. 4. Comparison of experimental and theoretical results.

stagnation region. Similar plots, not shown here, are obtained for various Reynolds numbers.

(B) *Discontinuous flow between tubes*

As the distance between the tube is increased to $H = 0.4$ and 0.6 cm, a fractionated film is obtained. Thus, the tubes are now "connected" by fragments of a liquid sheet which seem to migrate horizontally to and from in between the tubes. A further increase in the distance to $H \geqslant 1.0$ cm brings about the formation of dripping sites wherefrom the solution is distributed over the test tube in the form of successive drops.

to the onset of turbulence, consistent with continuous film characteristics. The transition of the discontinuous feed is of greater interest. Here, the unsteady nature of the dripping phenomena disappears as the drop trains turn into continuous jets. Under these conditions of high Re_N the film flow characteristics around the tube are evidently independent on whether the feed on top of the tube arrives as a continuous film or as a number of stable jets.

The experimental results presented so far were obtained by time-averaging the instantaneous values at the measurement points. A typical record of the

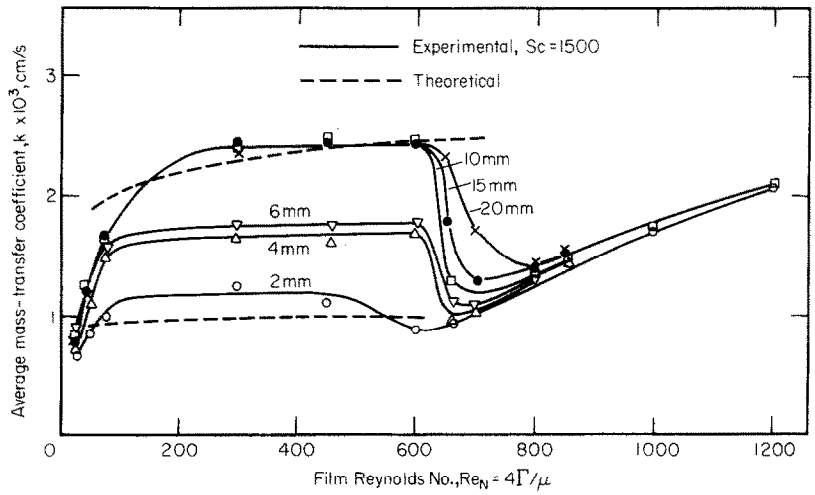

FIG. 5. Effect of flow rate and distance between tubes on the average mass-transfer coefficient.

The spatial and temporal average mass-transfer coefficients for the whole range of distances between the tube are shown in Fig. 5. For completeness, the figure includes the curve for continuous feed obtained at $H = 0.2$ cm. As is indicated in this figure, the transfer rates are enhanced as a segmental sheet is formed and are further intensified in the region of dripping. However, no further increase in the transfer rates are noticed as the tube distance increases beyond $H = 1.0$ cm.

Also included in Fig. 5 are the theoretical curves obtained by utilizing equation (23) for simulating the dripping and equation (13) for the smoothly cascading film. Evidently, the data for the intermediate region, of 0.4–0.6 cm lies in between the two limiting theoretical curves.

With reference to Fig. 5, it is instructive to note the effect of the flow rate on the transfer coefficient. The initial increase of the transfer coefficient at low Re_N for all values of H is attributed to the establishment of a uniform continuous film over the surface of the tube. For $Re_N > 100$, the transfer coefficient is practically constant up to $Re \simeq 600$. This is consistent with the above analysis which predicts but a slight effect of film flow rate on the transfer coefficient. However, further increase of the flow rate shows a decrease followed by a moderate increase of the transfer coefficient. This transition of the continuous film is most probably due

local instantaneous mass-transfer coefficient is demonstrated in Fig. 6. It is seen that with intermittent feed the mass-transfer rates have a complicated periodical relationship, due to the effect of local flow disturbances. These disturbances are random, here assumed to be ergodic, and the raw signals were processed utilizing probabilistic functions of first and second orders (mean value, auto-correlation function and power density spectrum) [12]. The evaluation of the data was done numerically, with data samples taken at time interval of about 20 ms utilizing an analog–digital converter and an online realtime PDP/8 Digital computer. The periodic nature of the transport phenomena was definitely established.

The periodic nature of the transfer coefficient is evident in Fig. 7, where the power spectrum density function is plotted for various points along the periphery. As seen in Fig. 7, the low frequencies of 2–3 Hz predominate and persist over the circumference, while the higher frequencies, evident at the top stagnation region, decay with the tangential distance.

As seen in Figs. 6 and 7, the strongly noticeable transient effects at the stagnation point decay along the periphery. Figure 8 represents the relative fluctuation of the local mass transfer coefficient at various Reynolds number. As is indicated by the curves, the amplitude fluctuation is highest at the top and bottom of the tube. This is expected in view of the drop

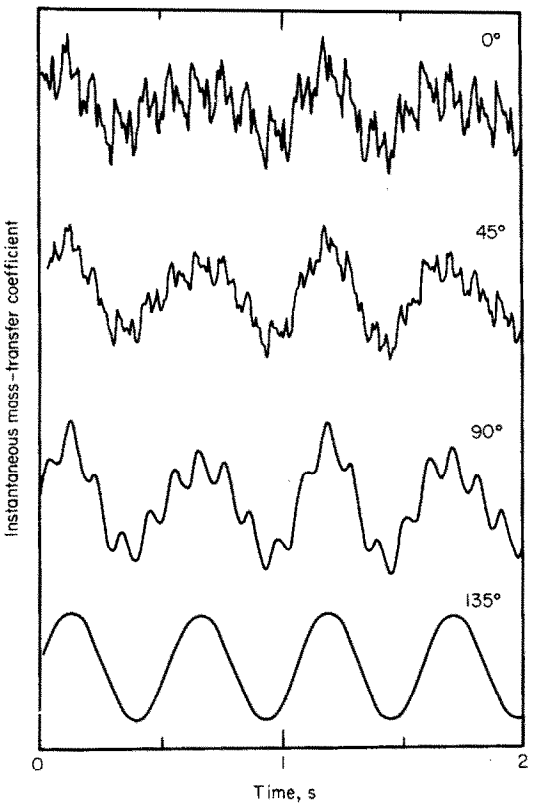

FIG. 6. Instantaneous local mass-transfer coefficients at different points along the periphery of a smooth tube; $Re_N = 200$, $H = 10$ cm.

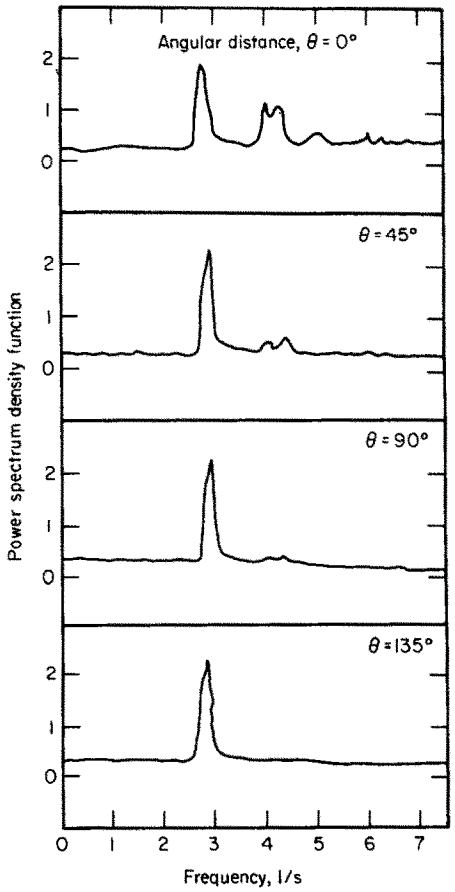

FIG. 7. Power spectrum density function of local mass-transfer coefficient.

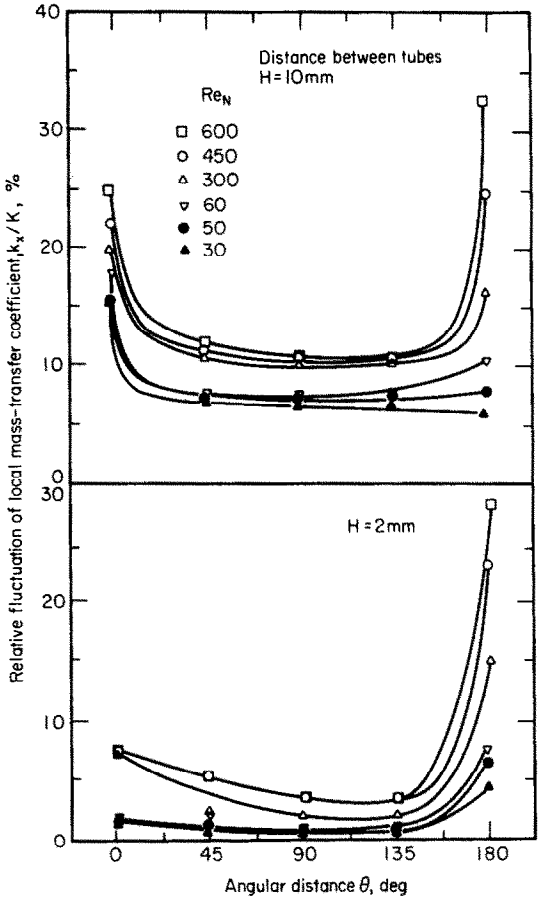

FIG. 8. Fluctuations of local mass-transfer coefficient, relative to local mean value, at various film flow rates.

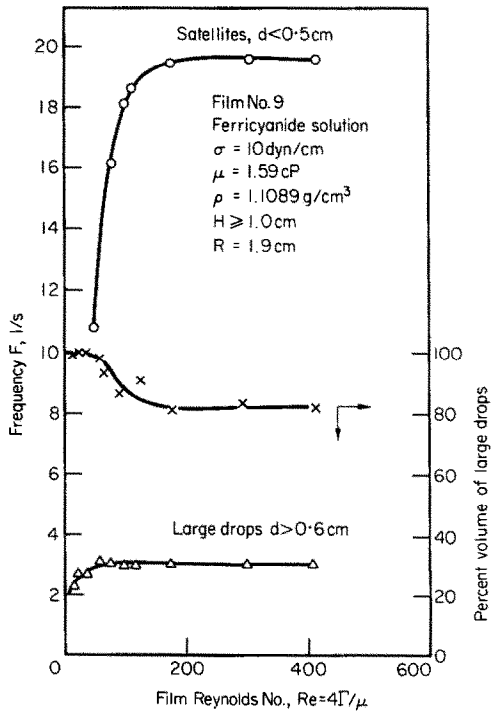

FIG. 9. Effect of film flow rate on the frequency and volumetric distribution of the drops.

impingement at the top and drops detachment at the bottom of the tube. Obviously, the latter is independent of the mode of fluid flow between the tubes. However, these are highly localized effects which decay rapidly outside the stagnation regions, and thus their influence on the spatial mean coefficient is practically negligible.

In order to establish a relationship between the dripping characteristics and the instantaneous mass transfer rate, a cine-camera operating at 68 fps was used to photograph the falling droplet trains between the feeder and test tubes. The frequency and size of drops as well as the distance between the active sites which produce the drops were measured from the projected ($\times 40$) image of the frames.

Typical dripping characteristics are shown in Figs. 9 and 10. At the $Re_N < 100$ range, the frequency of the drops increases and the distance between neighboring drop-formation sites decreases as the flow rate is increased. Two types of drops are distinguished at $Re_N > 100$: large, $d > 6$ mm drops which are followed by relatively small droplets—satellites—of various sizes and higher frequency. However, the frequencies of both the large and small drops remain constant for $Re_N > 150$. Note that in the normal operating range, the large drops represent some 80 vol% of the total flow rate.

Figure 10 represents the dependence of the average distance between active sites on the Reynolds number. For $Re_N > 150$ the horizontal spacing of these sites remains practically constant. It is interesting to note that the cine camera studies reveal that the number and location of these sites are unchanged even for the lower flow rates. However, since the total flow at low flow rates is not sufficient to "feed" and generate drops at all these sites, the sites are alternatively active. Thus the observed average distance between simultaneously active sites seen to be disproportionately large in the low Reynolds regime. As the film flow rate is increased, more sites are seen to be simultaneously active, and complete wettability of the test-tube is obtained as Re_N reaches a value of 100–150. Also, the frequency of the drops and, correspondingly, the mass + transfer coefficient are stabilized.

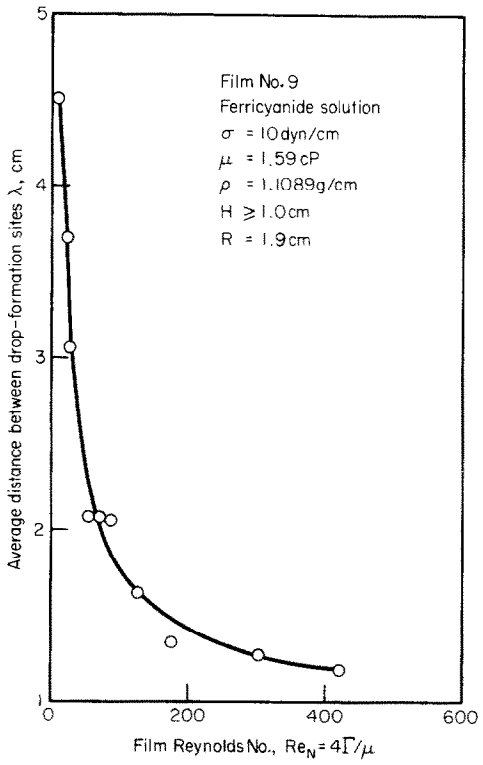

FIG. 10. Effect of film flow rate on the average distance between drop formation sites.

Inspection of Figs. 7 and 10 indicates that the main frequency of the mass transfer coefficient practically coincides with the frequency of the large drops. This is well understood in view of the fact that large drops falling on a liquid interface penetrate deeper than smaller ones [13]. In the case under consideration $Sc \gg 1$ and one can comfortably conclude that the large, low frequency, drops which penetrate into the liquid film control the transfer rate, whereas the small drops, with high frequencies, have but a slight effect on the overall average transfer rate.

Finally, it is perhaps relevant to emphasize that the effect of the small, high frequency, drops on the mass-transfer rate at the high Schmidt numbers discussed here will not be negligible in the case of heat and mass transfer with fluids of small Prandtl or Schmidt numbers.

CONCLUSIONS

1. The electrochemical experimental technique developed here has proved to be very sensitive and reliable for the study of mass-transfer rates from/to thin films around horizontal tubes. Analog–digital conversion of instantaneous signals enabled the detailed analysis of the local, spatial and temporal average characteristics.

2. The effect of flow rate and vertical distance between tubes has been elucidated. Essentially, four characteristic regimes were identified: (a) Continuous smooth film flow between the tubes, (b) rivulated films flowing between the tubes, (c) drops falling between the tubes, (d) continuous jets flowing between the tubes.

3. Dripping between tubes enhances the transfer rate by a factor of about two as compared to smooth film flow.

4. The dependence of the transfer coefficient on the flow rate is practically negligible at the high Schmidt values considered here.

5. The theoretical analysis gave good agreement with the experimental data for smooth film flow and dripping between the tubes. These cases represent the lower and upper bounds of the transfer coefficients.

6. Cine-camera studies showed that approximately 80% of the volumetric flow rate between the tubes occurs by low frequency, large diameter, drops. The frequency of these large drops coincides with the predominating frequency exhibited by the instantaneous mass transfer coefficients.

Acknowledgement—This research was supported by a grant from the United States–Israel Binational Science Foundation (BSF), Jerusalem, Israel.

The authors wish to thank Prof. A. E. Dukler, University of Houston, Texas, for many exciting discussions and useful suggestions in the course of this work. Thanks are also due to Prof. A. Solan, Dept. of Mech. Engng, Technion, for providing the initial facilities and advice in the preliminary stages of this study.

REFERENCES

1. D. Moalem and S. Sideman, Theoretical analysis of a horizontal condenser–evaporator tube, *Int. J. Heat Mass Transfer* **19**(3), 259 (1976).
2. D. Moalem and S. Sideman, Theoretical analysis of a horizontal condenser–evaporator elliptical tube, *J. Heat Transfer* **97**, 352 (1975).
3. S. Sideman, D. Moalem and R. Semiat, Theoretical analysis of conduits of various cross sections, *Desalination J.* **17**, 167 (1975).
4. S. Sideman, D. Moalem and R. Semiat, Performance improvement of horizontal evaporator–condenser desalination units, in *Proceedings of the 5th International Symposium on Fresh Water from the Sea, Alghero, Sardinia, Italy*, Paper 70-2.7 (May 1976).
5. T. Mizushina, The electrochemical method in transport phenomena, *Adv. Heat Transfer* **7**, 87 (1971).
6. H. Horn, Enhancing transfer rates: transport characteristics of films flowing over horizontal tubes of various surface configurations, M.Sc. Chem. Eng. thesis (in Hebrew), Technion—IIT (March 1976).
7. H. Schlichting, *Boundary Layer Theory* 6th edn, pp. 89, 271, 285. McGraw-Hill, New York (1968).
8. A. Zfati, Heat transfer in laminar flow of a liquid film on a horizontal cylinder, M.Sc., Mech. Eng. thesis (in Hebrew), Technion–Israel Inst. Tech. (1971).
9. A. Solan and A. Zfati, Heat transfer in laminar flow of a liquid film on a horizontal cylinder, in *Proceedings of the 5th International Heat Transfer Conference, Tokyo, Heat Transfer* 1974, FC2.9, Vol. 2, p. 90. JSME SCEJ, Tokyo (1974).
10. H. Kramers and P. J. Kreyger, Mass transfer between a flat surface and a falling liquid film, *Chem. Engng Sci.* **6**, 42 (1956).
11. D. R. Oliver and T. E. Atherinos, Mass transfer to liquid films on an inclined plane, *Chem. Engng Sci.* **23**, 525 (1968).
12. S. Sideman and H. Horn, Enhancing transfer rate: transport characteristics of films flowing over horizontal tubes of various surface configurations, Proj. 071–152, to U.S.–Israel Binational Science Foundation, Technion R & D Found. Ltd., Haifa, Israel, Reports No. 37 (Oct. 1974) and No. 40 (March 1975).
13. S. Hartland, S. Ramakrishnan and R. W. Hartley, The oscillation of drops and spheres at fluid–liquid interfaces, *Chem. Engng Sci.* **30**, 1141 (1975).

CARACTERISTIQUES DE TRANSPORT DES FILMS COULANT SUR DES TUBES LISSES HORIZONTAUX

Résumé—Une technique électrolytique utilisant une solution de ferrocyanure et de ferricyanure de potassium donne les flux locaux de transfert entre en film et un tube horizontal. Une conversion analogique—digitale permet l'analyse détaillée des caractéristiques locales, spatiales et temporelles du transfert. Le flux transféré dépend du mode d'alimentation du liquide. On identific quatre régimes caractéristiques de transfert qui dépendent du débit et de la distance entre le tube d'essai et le tube d'alimentation en liquide: (1) film lisse et continu entre les tubes, (2) écoulement du film avec rides, (3) formation de gouttes entre les tubes, (4) jets continus entre les tubes. Les gouttes entre les tubes s'accompagnent d'un accroissement du transfert selon un facteur égal à deux par rapport au cas du film lisse. Une analyse théorique donne un bon accord avec les données expérimentales dans le cas des films lisses jusqu'au phénomène de formation des gouttes.

TRANSPORTCHARAKTERISTIKEN EINES RIESELFILMS AN HORIZONTALEN GLATTEN ROHREN

Zusammenfassung—Ein elektronisches Verfahren ergibt, unter Verwendung der Auflösung von Kaliumeisenzyanür—Kaliumeisenzyanid, zuverlässig die momentane örtliche Übergangsrate zwischen einem Film und einem horizontalen Rohr. Analog-Digital-Umsetzung ermöglicht eine ausführliche Analyse der lokalen, räumlichen und zeitlichen Transportcharakteristiken. Die Übertragungsrate hängt, so wurde gefunden, von der Art der Flüssigkeitsaufgabe ab. Als Haupteinflußgrößen sind die Berieselungsmenge und der Abstand zwischen Versuchsrohr und Berieselungsrohr vorhanden. Daneben wurden vier charakteristische Bereiche festgestellt: (1) kontinuierliche glatte Filmströmung zwischen den Rohren, (2) wellige Filmströmung, (3) Herabtropfen zwischen den Rohren, (4) kontinuierlich strömende Strahlen zwischen den Rohren. Es wurde gefunden, daß das Herabtropfen zwischen den Rohren die Übertragungsrate um den Faktor zwei erhöht gegenüber der glatten Filmberieselung. Eine theoretische Untersuchung ergab eine gute Übereinstimmung mit den experimentellen Ergebnissen für den unteren Bereich des glatten Rieselfilmes und den oberen Bereich des Herabtropfens.

ХАРАКТЕРИСТИКИ ПЕРЕНОСА ПЛЕНОК ПРИ ТЕЧЕНИИ В ГОРИЗОНТАЛЬНЫХ ГЛАДКИХ ТРУБАХ

Аннотация — С помощью электрохимического метода, основанного на использовании раствора калиевая соль железистосинеродистой кислоты — калиевая соль железистосинеродистой кислоты, получены довольно точные значения локальных мгновенных интенсивностей переноса между пленкой и поверхностью горизонтальной трубы. Аналого-цифровые преобразования

позволили провести тщательный анализ локальных и пространственно-временных характеристик переноса.

Найдено, что скорость переноса зависит от способа подачи жидкости. В зависимости от расхода жидкости и расстояния между рабочей трубой и трубой, подводящей жидкость, выделены четыре характерных режима переноса: (1) непрерывное безволновое пленочное течение между трубами; (2) ручейковое пленочное течение; (3) проточное течение между трубами; (4) непрерывное струйное течение между трубами. Найдено, что проточное течение между трубами в два раза увеличивает скорость переноса по сравнению с безволновым пленочным течением.

Теоретический анализ показал хорошее совпадение с экспериментальными данными для безволнового пленочного течения у нижней границы и проточного у верхней.